Scientific paper

Syntheses, Crystal Structures and Characterization of Two New Lanthanide Mercury Halide Compounds

Xi-Yu Shao, Hao-Dong Liu, Long-Hua Zeng, Yu-Yue Xu, Wen-Tong Chen*, Cheng Liu*, Sheng-Ping Dai and Chang-Wang Pan

School of Chemistry and Chemical Engineering, Ji'an Key Laboratory of Photoelectric Crystal Materials and Device, Key Laboratory of Jiangxi Province for Special Optoelectronic Artificial Crystal Materials, Humic Acid Utilization Engineering Research Center of Jiangxi Province, Institute of Applied Chemistry, Jinggangshan University, 343009, Ji'an, Jiangxi, China

* Corresponding author: E-mail: wtchen_2000@aliyun.com (W.-T. Chen); 234871279@qq.com (C. Liu) Tel.: +86(796)8100490; fax +86(796)8100490

Received: 08-17-2024

Abstract

Two new lanthanide mercury halide compounds with isonicotinic acid as a ligand, namely, $[Gd(\mu_2-HIA)_2(\mu_3-IA)(H_2O)_2(HgCl_2)]_n(nHgCl_4)\cdot 3nH_2O$ (1) (HIA = isonicotinic acid) and $\{[Nd(\mu_2-HIA)_3(DMF)(H_2O)]_n\}[(Hg_4Br_{11})_n](2HgBr_2)(nBr)\cdot nH_3O$ (2), were synthesized with solvothermal reactions and characterized by single-crystal X-ray diffraction. Compound 1 is characterized by a two-dimensional (2-D) layer-like structure, while compound 2 features a one-dimensional (1-D) chain-like structure. The lanthanide ions in both compounds are eight coordinated and show a square antiprism geometry. The mercury ions exhibit various coordination motifs. Compound 1 exhibits ultraviolet upconversion photoluminescence emission, whereas compound 2 displays red photoluminescence. The photoluminescence emissions arise from the characteristic 4*f* electron intrashell transitions of the ${}^6P_{7/2} \rightarrow {}^8S_{7/2}$ of the Gd³⁺ ions in compound 1 and the ${}^4F_{9/2} \rightarrow {}^4I_{9/2}$, ${}^4F_{7/2} + {}^4S_{3/2} \rightarrow {}^4I_{9/2}$, ${}^4F_{5/2} + {}^2H_{9/2} \rightarrow {}^4I_{9/2}$, of the Nd³⁺ ions in compound 2. Compound 2 has CIE (Commission Internationale de l'Éclairage) chromaticity coordinates of (0.7142, 0.2857) and its CCT (correlated color temperature) is 138,224 K. Solid-state UV/Vis diffuse reflectance spectra revealed that the semi-conductor band gaps of the compounds are 3.12 eV and 3.23 eV, respectively. Elemental analyses and FT-IR spectroscopy were carried out to confirm the purity of the compounds.

Keywords: gadolinium; band gap; neodymium; photoluminescence; solvothermal reaction

1. Introduction

Over the course of several decades, lanthanide coordination compounds have increasingly garnered interest from researchers in chemistry and materials science. This heightened attention arises from the fact that these compounds often exhibit valuable physicochemical properties, including photoluminescence, catalytic activity, magnetic capabilities, and biochemical sensing abilities, thus making them highly sought-after for applications in displays, catalysis, medicine, and numerous other fields. 1-6 The intriguing physicochemical attributes of lanthanide coordination compounds primarily arise from the abundant 4f electrons present in the lanthanide ions. Among these properties, which are captivating, photoluminescence stands out as particularly fascinating. Lanthanide coordination compounds typically exhibit robust photoluminescence emission when 4f electron transitions occur efficiently. To explore their potential applications in domains such as electrochemical displays, luminescent sensors, medicine, magnetic materials, light-emitting diodes, and more, extensive research has been conducted on lanthanide coordination compounds.^{7–12}

Zinc, cadmium, and mercury, classified as Group 12 elements, have garnered considerable attention for a multitude of reasons, including zinc's pivotal role in biological systems, the diverse coordination motifs they exhibit, as well as their enticing photoelectric and photoluminescence behaviors, among others. ^{13–16} Furthermore, the Group 12 elements also hold potential for use in the synthesis of semiconductor materials, and numerous semiconductor materials incorporating these elements have been documented to date. ^{17–20}

Organic molecules featuring diverse functional groups are invaluable in the synthesis of metal coordina-

tion compounds. Specifically, N-containing heterocyclic molecules, such as isonicotinic acid, nicotinic acid, 4,4'-bipyridine, 2,2'-bipyridine, and others, have been extensively utilized in the preparation of these compounds due to their abundant coordination sites and versatility in coordination modes.^{21–23} To our understanding, isonicotinic acid serves as a valuable building block due to its unique structural features, namely, two carboxylic oxygen atoms on one side and a nitrogen atom on the other. This arrangement enables isonicotinic acid molecules to bind with various metal ions, facilitating the formation of novel compounds. Consequently, isonicotinic acid is regarded as an excellent chelating and bridging ligand for constructing metal coordination compounds with extended, high-dimensional structures. Additionally, the pyridyl ring in isonicotinic acid possesses delocalized π -electrons, which renders it a promising candidate for the development of luminescent materials in diverse fields, including organic light-emitting diodes (OLEDs), chemical sensors, solar energy conversion, and more. 24-26

For many years, our team has been aiming at research on photoluminescence and semiconductor compounds. $^{27-29}$ We have recently become interested in the design and preparation of lanthanide mercury halide compounds with new structural geometries and fascinating properties. In this paper, we report the syntheses, single crystal structures, FT-IR, and semiconductor bandgaps, as well as the photoluminescence, CIE, and CCT of two new lanthanide mercury halide compounds with isonicotinic acid as a ligand, namely, $[Gd(\mu_2-HIA)_2(\mu_3-IA)(H_2O)_2(Hg-Cl_2)]_n(nHgCl_4)\cdot 3nH_2O$ (1) and $[Nd(\mu_2-HIA)_3(DMF)(H_2O)]_n\}[(Hg_4Br_{11})_n](2HgBr_2)(nBr)\cdot nH_3O$ (2). Both compounds were synthesized via solvothermal reactions. It is noteworthy that compound 1 exhibits ultraviolet upconversion photoluminescence.

2. Experimental

2. 1. Instruments and Chemicals

All reagents and chemicals applied for the syntheses of the title compounds were commercially available and directly used. The elemental analyses of carbon, hydrogen and nitrogen were conducted on an Elementar Vario EL elemental analyzer. The FT - IR spectroscopy was carried out on a PE Spectrum - One FT - IR spectrophotometer with KBr pellets in the wavenumber of 4000 cm⁻¹ \sim 400 cm⁻¹. The photoluminescence spectra were measured on a F97XP photoluminescence spectrometer with 200 nm ~ 900 nm wavelength. The solid - state UV/Vis diffuse reflectance spectra (DRS) were carried out on a TU1901 UV/ Vis spectrometer with 190 nm ~ 900 nm wavelength. The band gap energy (E_g) of the title compounds was calculated from DRS data using the Kubelka-Munk equation $(\alpha h v = A(h v - E_g)^{1/2})$; where α is absorption coefficient; h is Planck constant, v is light frequency, A is Tauc's constant, and E_g is absorption coefficient. ³⁰

2. 2. Preparation of $[Gd(\mu_2\text{-HIA})_2(\mu_3\text{-IA})$ $(H_2O)_2(HgCl_2)]_n(nHgCl_4)\cdot 3nH_2O(1)$

The GdCl₃·6H₂O (1 mmol, 372 mg), HgCl₂ (2 mmol, 542 mg), isonicotinic acid (3 mmol, 369 mg) and distilled water (15 mL) were loaded into a 25 mL Teflon-lined stainless steel autoclave. This autoclave was kept at 473 K for seven days. After naturally cooling to room temperature, colorless block-like crystals suitable for the single-crystal X-ray diffraction measurements were obtained, washed with distilled water and dried in air. The yield was 35% (based on GdCl₃·6H₂O). C₁₈H₂₄Cl₆GdHg₂N₃O₁₁: calc. C, 17.58; H, 1.97; N, 3.42; Found C, 17.68; H, 1.99; N, 3.48. FT-IR peaks (cm⁻¹) of 1: 3514(vs), 3440(vs), 3206(w), 3134(m), 3073(s), 2892(w), 2803(w), 1699(m), 1590(vs), 1501(w), 1408(vs), 1230(m), 1077(w), 1048(m), 1004(w), 846(s), 761(vs), 676(s), 547(m) and 413(s). FT-IR peaks (cm⁻¹) of isonicotinic acid: 3453(vs), 3105(w), 3052(m), 2923(w), 2850(w), 2806(w), 1961(m), 1714(vs), 1613(s), 1565(m), 1476(w), 1411(s), 1335(s), 1302(w), 1229(s), 1140(m), 1023(s), 857(m), 764(s), 692(m), 671(w) and 485(m).

2. 3. Preparation of {[Nd(μ_2 -HIA)₃(DMF) (H₂O)]_n}[(Hg₄Br₁₁)_n](2HgBr₂) (nBr)·nH₃O (2)

The Nd(NO₃)₃·6H₂O (0.5 mmol, 218 mg), HgBr₂(2 mmol, 720 mg), isonicotinic acid (1.5 mmol, 185 mg), 1 mL DMF and 10 mL distilled water were loaded into a 25 mL Teflon-lined stainless steel autoclave. The autoclave was heated at 433 K for ten days and powered off. After naturally cooling to room temperature, yellow block-like crystals suitable for the single-crystal X-ray diffraction measurement were collected, washed with distilled water and dried in air. The yield was 23% (based on Nd(NO₃)₃·6H₂O). $C_{21}H_{27}Br_{16}Hg_6N_4NdO_9$: calc. C, 8.12; H, 0.88; N, 1.80; Found C, 8.20; H, 0.85; N, 1.87. FT-IR peaks (cm⁻¹): 3465(vs), 3081(w), 1618(s), 1590(s), 1408(s), 1380(vs), 1242(w), 1101(w), 1048(w), 842(w), 761(m), 681(m), 543(w) and 470(w).

2. 4. X-ray Single Crystal Structure Characterization

The X-ray single crystal data of complexes 1 and 2 were obtained from a Rigaku Mercury CCD X-ray diffractometer equipped with a graphite monochromated Mo-K α radiation source, and the radiation wavelength is 0.71073 Å. The measurement was carried out using the ω scan mode. The single crystal data reduction and empirical absorption correction were conducted using the CrystalClear software. The single crystal structures of complexes 1 and 2 were solved using the direct method with the Siemens SHELXTL^{**} Version 5 software packages. All non-hydrogen atoms were generated based on the subsequent dif-

Table 1: Crystallographic data and structural analyses for complexes 1 and 2

Compound	1	2 C ₂₁ H ₂₇ Br ₁₆ Hg ₆ N ₄ NdO ₉	
Formula	C ₁₈ H ₂₄ Cl ₆ GdHg ₂ N ₃ O ₁₁		
M_r	1229.53	3105.81	
Color and Habit	colorless block	yellow block	
Crystal size/mm	$0.23 \times 0.07 \times 0.05$	$0.14 \times 0.06 \times 0.04$	
Crystal system	Monoclinic	Monoclinic	
Space group	$P2_1/c$	$P2_1/c$	
a (Å)	9.7208(3)	9.7418(3)	
b (Å)	19.8355(7)	27.1490(9)	
c (Å)	17.1090(5)	21.4775(12)	
β (°)	101.521(3)	100.772(4)	
$V(Å^3)$	3232.44(18)	5580.3(4)	
Z	4	4	
$2\theta_{ m max}$ /°	50	50	
Reflections collected	18390	30735	
Independent, observed reflections (R_{int})	5712, 4737 (0.0276)	9756, 6788 (0.0444)	
$d_{\text{calcd.}}$ (g/cm ³)	2.526	3.697	
μ/mm^{-1}	12.054	28.854	
T/K	293(2)	293(2)	
F(000)	2268	5412	
R1, wR2	0.0317, 0.0629	0.1108, 0.3030	
S	1.037	1.051	
Largest and mean Δ/σ	0.001, 0.000	0.000, 0.000	
$\Delta \rho$ (max, min) (e/Å ³)	1.116, -1.081	6.358, -5.117	

ference electron density maps and refined anisotropically, while all hydrogen atoms were placed theoretically. The final single crystal structures of complexes $\mathbf{1}$ and $\mathbf{2}$ were refined using the full-matrix least-squares refinement on F^2 . Crystallographic data and structural analyses of complexes $\mathbf{1}$ and $\mathbf{2}$ are given in Table 1. Selected bond lengths and bond angles are shown in Table 2. Hydrogen bonding geometry (Å, °) are listed in Table 3.

3. Result and Discussions

Compound 1 was prepared by using GdCl₃·6H₂O, HgCl₂, isonicotinic acid and distilled water in a Teflon-lined stainless steel autoclave at 473 K under hydrothermal conditions. Compound 2 was synthesized by using Nd(NO₃)₃·6H₂O, HgBr₂, isonicotinic acid, DMF and distilled water in a Teflon-lined stainless steel autoclave at 433 K under hydrothermal conditions. It is known that the hydrothermal reaction with organic molecules is a powerful way for the preparation of novel compounds. Under hydrothermal conditions, the properties of water behave very different from normal conditions, namely, water is superheated with obviously lowered viscosity. Solids are easily extracted into this water and the diffusion rate of reagents increases under hydrothermal conditions. So, many reactions can occurred. Lee and co-authors reported a mercury bromide complex [Hg₄Br₆L₂][Hg₂Br₆] which was prepared by using a slow evaporation method of solution.31 Hu et al documented a mercury bromide complex

(TMP)(Hg₂Br₅)·0.5H₂O which was also obtained by using a slow evaporation method of solution.³² Song and co-authors reported a mercury bromide complex [Cu₂(bi-py)₄HgBr₄][Hg₂Br₆] which was also synthesized by using a slow evaporation method.³³

The FT-IR spectroscopy of compounds 1 and 2 were carried out under room temperature. The FT-IR bands of both compounds are dominantly located in the frequency span of $600 \sim 1700 \text{ cm}^{-1}$. The very strong intensity bands residing at 3440 cm⁻¹, 3514 cm⁻¹ and 3465 cm⁻¹ should be ascribed to the O-H asymmetric vibration of the water molecules. The bands locating at 1618 cm⁻¹ and 1590 cm⁻¹ could be assigned to the stretching and bent vibrations of the C-N bonds of the pyridyl rings of the isonicotinic acid ligands. The bands at 1501 cm⁻¹, 1408 cm⁻¹, 1380 cm⁻¹, 1242 cm⁻¹ and 1230 cm⁻¹ could be assigned to the C-O stretching vibrations of the pyridyl rings of the isonicotinic acid ligands. The bands residing in the span of 842 ~ 1101 cm⁻¹ should be ascribed to the bending vibration of the pyridyl rings of the isonicotinic acid ligands. The bands locating at 413 cm⁻¹ ~ 761 cm⁻¹ could be assigned to the stretching vibrations of the Hg-Cl/Br bonds.³⁴ The very strong band 1714 cm⁻¹ of the free ligand isonicotinic acid disappeared in the FT-IR spectroscopy of compounds 1 and 2. This verifies that the carboxylic groups of the isonicotinic acid molecules are coordinated with metal. It is in good line with the single-crystal X-ray diffraction results.

The single-crystal X-ray diffraction experiments showed that both title compounds crystallize in the space group $P2_1/c$ of the monoclinic system with four formula

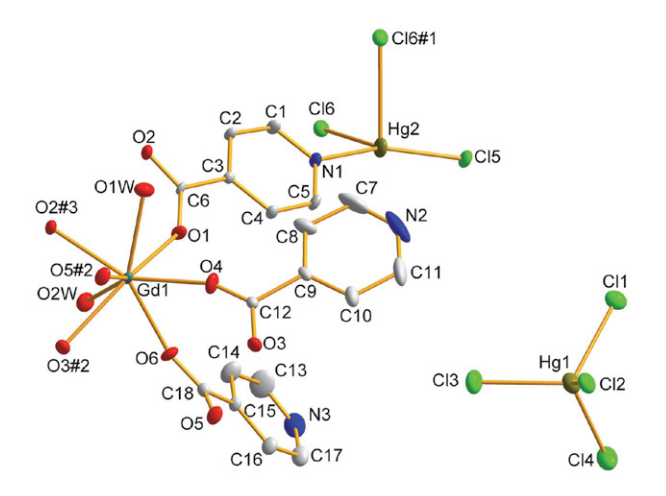


Fig. 1: An ORTEP figure of the asymmetric unit of complex 1 with 20% thermal ellipsoids. Lattice water molecules and hydrogen atoms were omitted for clarity.

molecules in each cell unit (Table 1). The crystallographically asymmetric unit of compound 1 consists of two Hg^{2+} cations, one Gd^{3+} cation, six Cl^- anions, two isonicotinic acid molecules, one isonicotinate anion, two coordination

water molecules and three lattice water molecules, as displayed in Fig. 1. All crystallographic independent atoms are located at general positions. The Gd3+ ions are bound by eight oxygen atoms: two from coordination water molecules, two from isonicotinic acid anions, and four from isonicotinic acid molecules, forming a GdO8 square antiprismatic geometry. As listed in Table 2, the Gd-O_{isonico-} tinic acid bond lengths of compound 1 locate in the span of 2.319(4) Å \sim 2.391(4) Å with an average value of 2.358(4) Å, while the Gd-O_{water} bond lengths are 2.438(4) Å and 2.499(4) Å. The Gd-O_{isonicotinic acid} bond lengths are obviously shorter than the Gd-O_{water} bond lengths. This suggests that the Gd3+ ions have much stronger affinity to the isonicotinic acid ligands than to the water molecules. These Gd-O bond lengths are in the normal span and comparable with the values documented in the references. 35,36 The O-Gd-O bond angles fall within the range of 69.60(15)° ~ 145.98(15)°.

The Hg1 ion is coordinated by four chloride ions to form an isolated HgCl₄ tetrahedron. The Hg2 ion is bound by one terminal chloride ion, two μ_2 -bridging chloride ions and one pyridine nitrogen atom to yield a distorted tetrahedron. The Hg–Cl bond lengths fall within the range

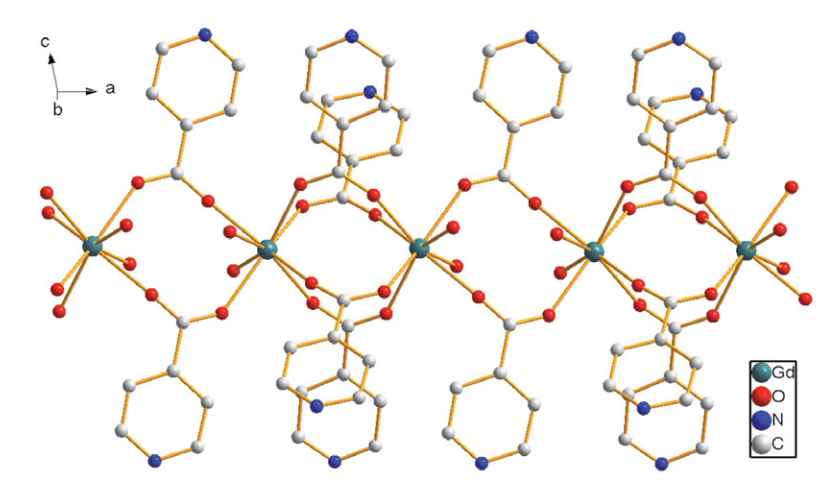


Fig. 2: A 1-D -Gd-(IA)₂-Gd-(HIA)₄-Gd- chain in complex 1

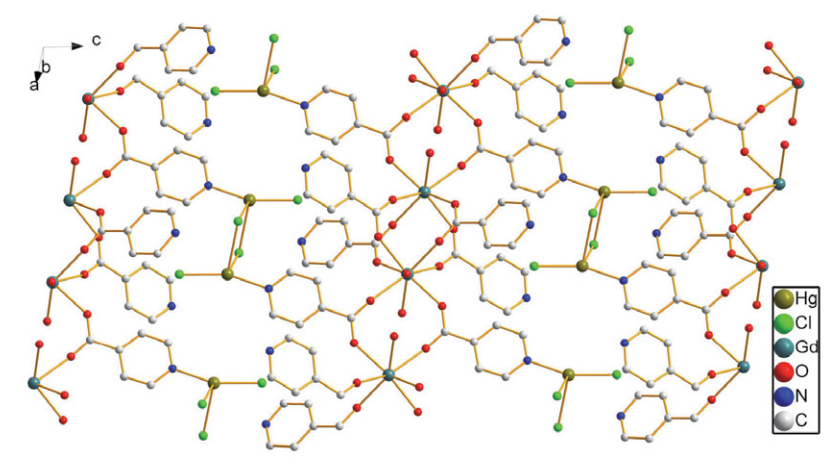


Fig. 3: A 2-D layer in complex 1

Table 2: Selected bond lengths (Å) and angles (°) of complexes 1 and 2

Complex 1					
Bond Lengths (Å)		Bond Angles (°)			
Hg(1)-Cl(1)	2.5081(18)	Cl(3)-Hg(1)-Cl(4)	112.03(8)		
Hg(1)-Cl(2)	2.5306(18)	Cl(3)- $Hg(1)$ - $Cl(1)$	115.60(7)		
Hg(1)-Cl(3)	2.438(2)	Cl(4)- $Hg(1)$ - $Cl(1)$	106.63(7)		
Hg(1)-Cl(4)	2.451(2)	Cl(3)-Hg(1)-Cl(2)	98.82(7)		
Hg(2)-N(1)	2.161(5)	Cl(4)-Hg(1)-Cl(2)	118.07(8)		
Hg(2)-Cl(5)	2.3205(16)	Cl(1)-Hg(1)-Cl(2)	105.82(6)		
Hg(2)-Cl(6)	2.7730(16)	N(1)-Hg(2)-Cl(5)	156.31(14)		
Hg(2)-Cl(6)#1	2.6795(17)	N(1)-Hg(2)-Cl(6)#1	97.53(13)		
Gd(1)-O(2)	2.319(4)	Cl(5)-Hg(2)-Cl(6)#1	102.80(6)		
Gd(1)-O(6)#2	2.336(4)	N(1)-Hg(2)-Cl(6)	92.48(13)		
Gd(1)-O(1)#3	2.358(4)	Cl(5)-Hg(2)-Cl(6)	100.46(5)		
Gd(1)-O(4)#2	2.361(4)	Cl(6)#1-Hg(2)-Cl(6)	87.26(5)		
Gd(1)-O(5)	2.388(4)	Hg(2)#1-Cl(6)-Hg(2)	92.74(5)		
Gd(1)-O(3)	2.391(4)	O(2)-Gd(1)-O(4)#2	145.98(15)		
Gd(1)-O(1W)	2.438(4)	O(5)-Gd(1)-O(1W)	69.60(15)		
Gd(1)-O(2W)	2.499(4)				

Symmetry transformations used to generate equivalent atoms: #1-x, -y+1, -z-1; #2-x, -y+1, -z; #3-x+1, -y+1, -z

Complex 2					
Bond Lengths (Å)		Hg(5)-Br(1) #1	3.298(5)		
Hg(1)-Br(1)	2.70(5)	Hg(6)-Br(14)	2.41(2)		
Hg(1)-Br(2)	2.38(5)	Hg(6)-Br(15)	2.416(15)		
Hg(1)-Br(3)	2.60(6)	Nd(1)-O(3)	2.36(5)		
Hg(1)-Br(5)	3.228(6)	Nd(1)-O(5)	2.39(4)		
Hg(2)-Br(3)	3.10(2)	Nd(1)-O(2)	2.39(5)		
Hg(2)-Br(4)	2.39(2)	Nd(1)-O(6)	2.42(5)		
Hg(2)-Br(5)	2.406(18)	Nd(1)-O(4)#2	2.45(5)		
Hg(2)-Br(6)	3.214(18)	Nd(1)-O(1)#2	2.46(5)		
Hg(3)-Br(7)	2.343(19)	Nd(1)-O(1W)	2.51(5)		
Hg(3)-Br(8)	2.373(18)	Nd(1)-O(7)	2.52(4)		
Hg(4)-Br(6)	2.646(18)	Bond Angles (°)			
Hg(4)-Br(9)	2.860(18)	Br(9)-Hg(3)-Br(1)#3	89.1(5)		
Hg(4)-Br(10)	2.455(16)	Br(14)-Hg(6)-Br(15)	176.9(9)		
Hg(4)-Br(11)	2.623(19)	Hg(1)-Br(3)-Hg(2)	89.4(15)		
Hg(5)-Br(12)	2.33(5)	Hg(4)- $Br(9)$ - $Hg(3)$	166.64(5)		
Hg(5)-Br(12)#1	3.144(5)	O(6)#1-Nd(1)-O(1)#2	145.3(18)		
Hg(5)-Br(13)	2.41(2)	O(6)#1-Nd(1)-O(1W)	72.0(16)		

Symmetry transformations used to generate equivalent atoms: #1 - x - 1, -y + 3, -z + 4; #2 - x, -y + 3, -z + 4; #3 x + 1, y, z.

of 2.3205(16) Å \sim 2.7730(16) Å with an average value of 2.5287(18) Å, while the Hg–N bond length is 2.161(5) Å. The Hg–Cl and Hg–N bond lengths are within normal ranges and comparable with the values documented in the references. 37,38 The Cl–Hg–Cl and N–Hg–Cl bond angles locate in the range of 87.26(5)° \sim 118.07(8)° and 92.48(13)° \sim 156.31(14)°, respectively. Two neighboring Hg(2) ions are linked by two μ_2 -bridging chloride ions to form a Hg₂Cl₄ moiety. The Hg(2)#1-Cl(6)-Hg(2) bond angle is 92.74(5)° that is close to a right angle. The neighboring Gd $^{3+}$ ions are interbridged together alternately by two isonicotinic acid anions and four isonicotinic acid molecules, to yield

a one-dimensional (1-D) chain running along the a axis, as shown in Fig. 2. The distances are 4.533 Å and 5.220 Å between adjacent $Gd^{3+}\cdots Gd^{3+}$ ions. The 1-D chains are connected by Hg_2Cl_4 moieties to form a two-dimensional (2-D) layer extending along the ac plane, as presented in Fig. 3. The deviation of the six atoms of the pyridyl rings of the three isonicotinic acid are in the range of -0.011 Å ~ 0.010 Å, -0.009 Å ~ 0.006 Å and -0.009 Å ~ 0.014 Å, respectively. Such small deviation suggests that each of the pyridyl rings of the three isonicotinic acid are almost coplanar. The torsion angles from the carboxylic groups to the pyridyl rings are $170.5(5)^{\circ}$, $168.2(5)^{\circ}$, $-173.3(5)^{\circ}$,

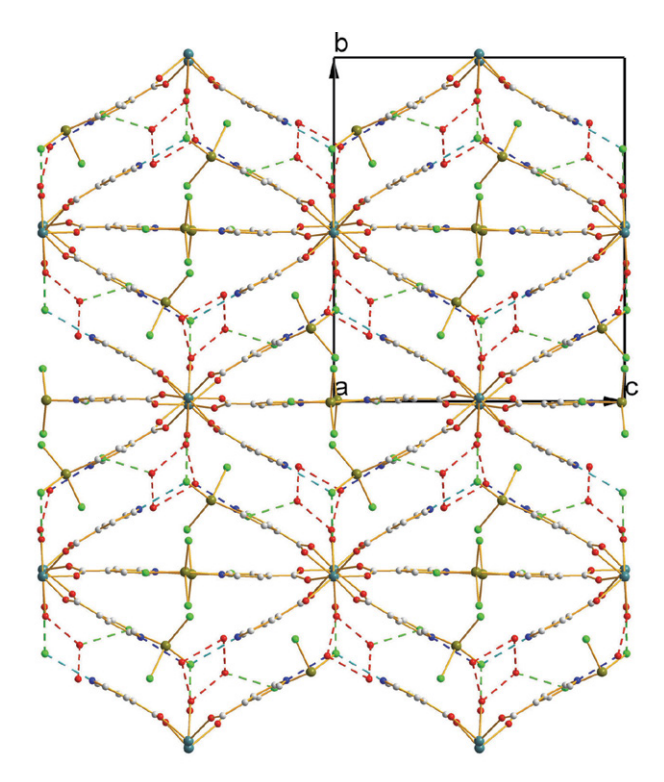


Fig. 4: The packing structure of complex **1** with the dashed lines representing hydrogen bonding interactions

 $-178.0(5)^{\circ}$, $-173.7(5)^{\circ}$ and $-169.8(5)^{\circ}$, respectively. The neutral isonicotinic acid molecule acts as a μ_2 -bridging ligand with two oxygen atoms binding to two Gd³⁺ cations, while the isonicotinic acid anion acts as a μ_3 -bridging ligand with two oxygen atoms binding to two Gd³⁺ cations and one nitrogen atom linking to one Hg²⁺ cation (see Fig. 3). There are eight hydrogen bonding interactions which can be grouped into five types, namely, O-H···O, N-H···Cl, O-H···Cl, N-H···O and C-H···Cl, as shown in Table 3. These hydrogen bonding interactions solidify the crystal packing

structure and construct a three-dimensional (3-D) supramolecular framework of complex 1, as presented in Fig. 4.

The single-crystal X-ray diffraction analysis results revealed that the crystallographically asymmetric unit of complex 2 is comprised of six Hg²⁺ cations, one Nd³⁺ cation, sixteen Br⁻ anions, three neutral isonicotinic acid molecules, one DMF molecule, one coordination water molecule and one lattice water molecule, as displayed in Fig. 5. All crystallographic independent atoms are located at general positions. The six crystallographically independent Hg²⁺ cations have two kinds of coordination geometries. The Hg1, Hg2, Hg4 and Hg5 ions are bound by four bromide ions to yield distorted tetrahedra. The Hg3 and Hg6 ions are coordinated by two terminal bromide ions to give a linear motif with the bond angles of Br(7)-Hg(3)-Br(8)and Br(14)-Hg(6)-Br(15) being of 169.2(9)° and 176.8(6)°, respectively. The Hg-Br bond lengths fall within the range of 2.33(5) Å \sim 3.298(5) Å. The Hg–Br bond lengths are in the normal span and comparable with the values reported in the references.^{39,40} The Br-Hg-Br bond angles fall within the range of 89.1(5)° ~ 176.9(9)°, while Hg-Br-Hg bond angles reside in the span of 89.4(15)° ~ 166.64(5)°. The Hg1, Hg2, Hg4 and Hg5 ions are connected by the μ_2 -bridging bromide ions to form a 1-D –Hg–Br–Hg–Br– Hg– chain running along the *a* axis, as shown in Fig. 6. Lee and co-authors reported a mercury bromide complex with two rhomboidal clusters [Hg₂Br₆]^{2-.31} Hu et al reported a complex (TMP)(Hg₂Br₅)·0.5H₂O containing a (Hg₂Br₅)⁻ anion.³² Song and co-authors reported a mercury bromide complex [Cu₂(bipy)₄HgBr₄][Hg₂Br₆] that contains a $[Hg_2Br_6]^{2-}$ anion.³³

The Nd^{3+} ion is surrounded by eight oxygen atoms, of which one is offered by one coordination water molecule, one comes from one DMF molecule, six are offered by six isonicotinic acid molecules, to yield a NdO_8 square antiprismatic geometry. As shown in Table 2, the Nd - $\mathrm{O}_{\mathrm{isonicotinic}\,\mathrm{acid}}$ bond lengths of compound 1 fall within

Table 3: Hydrogen bonding geometry (Å, deg) of complexes 1 and 2

	Complex 1			
D-H···A	D-H	HA	D···A	D-HA
$O2W-H2WA\cdotsO3W(-x, -1/2+y, -1/2-z)$	0.82	2.16	2.971(7)	169
N2-H2B···Cl1(-1+x, 1/2-y, -1/2+z)	0.86	2.53	3.269(10)	145
O1W-H1WB···Cl1(1-x, 1-y, -z)	0.90(5)	2.30(5)	3.158(4)	159(7)
N3-H3AO3W	0.86	1.98	2.795(9)	159
O5W-H5WA···Cl3(x, 1/2-y, 1/2+z)	0.94(9)	2.62(10)	3.118(9)	114(10)
O3W-H3WA···O4W($-x$, $1/2+y$, $-1/2-z$)	0.90(4)	2.23(3)	3.000(16)	144(2)
C17-H17A···Cl3(1-x, 1/2+y, -1/2-z)	0.93	2.80	3.434(9)	126
C13-H13A···Cl2 (-x, 1/2+y, -1/2-z)	0.93	2.79	3.468(10)	131
	Compound	2		
D-H···A	D-H	H···A	D···A	D-H···A
C7-H7A···Br2(-1-x,1/2+y,7/2-z)	0.94	2.92	3.80(8)	158

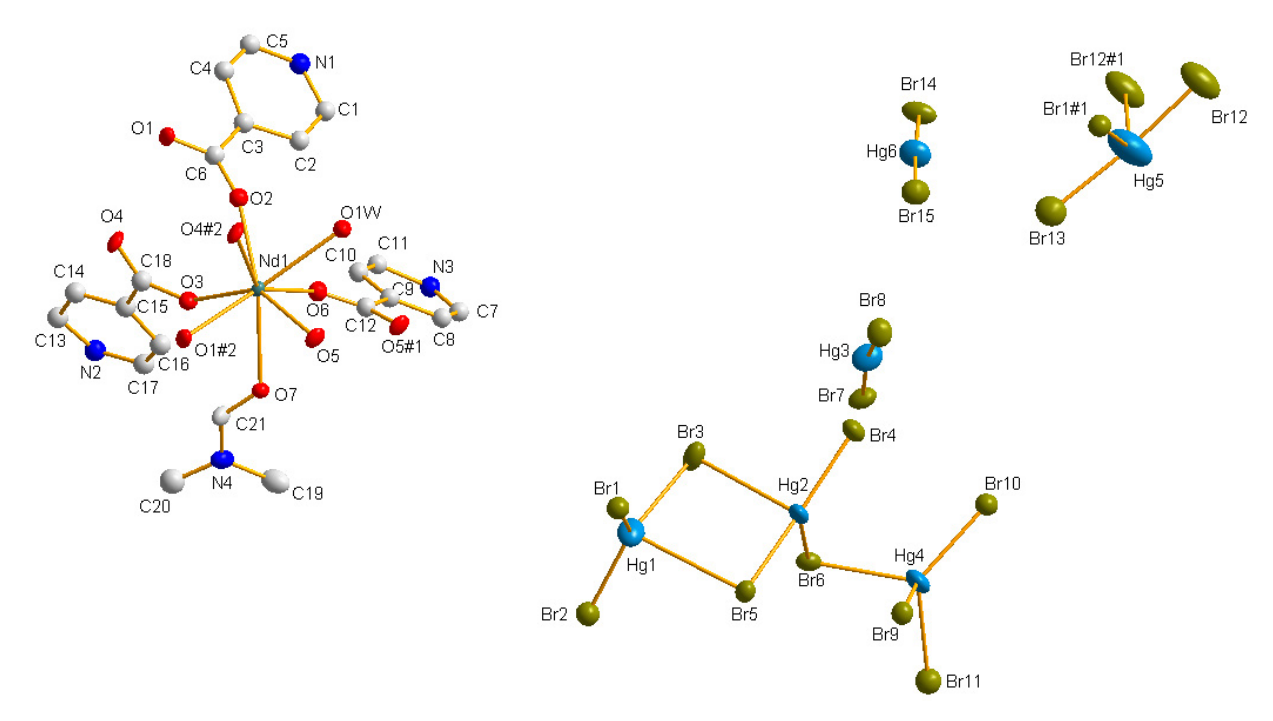


Fig. 5: An ORTEP drawing of complex 2 with 20% thermal ellipsoids. Lattice water molecules, isolated bromide ions, disordered atoms and hydrogen atoms were omitted for clarity.

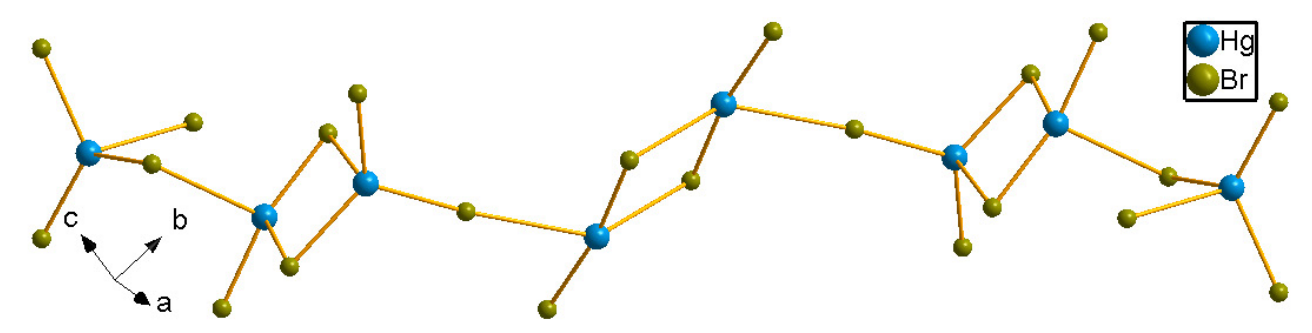


Fig. 6: A 1-D -Hg-Br-Hg-Br-Hg- chain in complex ${\bf 2}$

the range of 2.36(5) Å \sim 2.46(5) Å with an average value of 2.41(5) Å, while the Nd-O_{water} and Nd-O_{DMF} bond lengths are 2.51(5) Å and 2.52(4) Å, respectively. The Nd- $O_{isonicotinic\ acid}$ bond length is the shortest and the Nd- O_{DMF} bond length is the longest. This suggests that the Nd³⁺ ion has much more stronger affinity to the isonicotinic acid ligands than to the DMF molecules. These Nd-O bond lengths lie in the normal range and comparable with the values documented in the references. 41,42 The O-Nd-O bond angles fall within the range of $72.0(16)^{\circ} \sim 145.3(18)^{\circ}$. The neighboring Nd³⁺ ions are interbridged together alternately by two and four isonicotinic acid molecules, to form a one-dimensional (1-D) -Nd-(HIA)₄-Nd-(HIA)₂-Nd- $(HIA)_4$ -Nd- chain running along the a axis, as shown in Fig. 7. The distances are 4.639 Å and 5.141 Å between adjacent Nd³⁺...Nd³⁺ ions. All of the isonicotinic acid molecule acts as a μ_2 -bridging ligand with two oxygen atoms binding to two Nd³⁺ cations (see Fig. 7). The deviation of the six

atoms of the pyridyl rings of the three isonicotinic acid are in the range of $-0.042 \text{ Å} \sim 0.061 \text{ Å}$, $-0.060 \text{ Å} \sim 0.047 \text{ Å}$ and −0.029 Å ~ 0.026 Å, respectively. Such small deviation suggests that each of the pyridyl rings of the three isonicotinic acid are almost coplanar. The torsion angles from the carboxylic groups to the pyridyl rings are 174.6(7)°, 167.7(7)°, -172.2(7)°, -174.9(7)°, -172.8(5)° and -177.9(4)°, respectively. There is only one hydrogen bonding interaction in compound 2, namely, C7-H7A···Br2(-1-x,1/2+y,7/2-z). This hydrogen bonding interaction connects the above mentioned 1-D -Hg-Br-Hg-Br-Hg- chains and -Nd-(HIA)₄-Nd-(HIA)₂-Nd-(HIA)₄-Nd- chains together to yield a 2-D supramolecular layer extending along the ac plane, as shown in Fig. 8. Hydrogen bonding interactions and electrostatic forces enhance the stability of the crystal packing structure of complex 2, as presented in Fig. 9.

It is well-known that a large number of lanthanide and mercury complexes can display photoluminescence

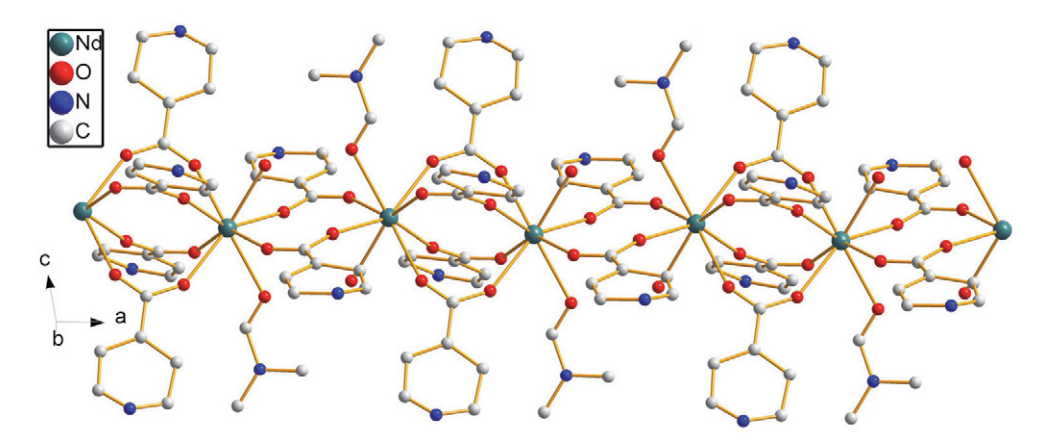


Fig. 7: A 1-D -Nd-(HIA)₄-Nd-(HIA)₂-Nd-(HIA)₄-Nd- chain in complex 2

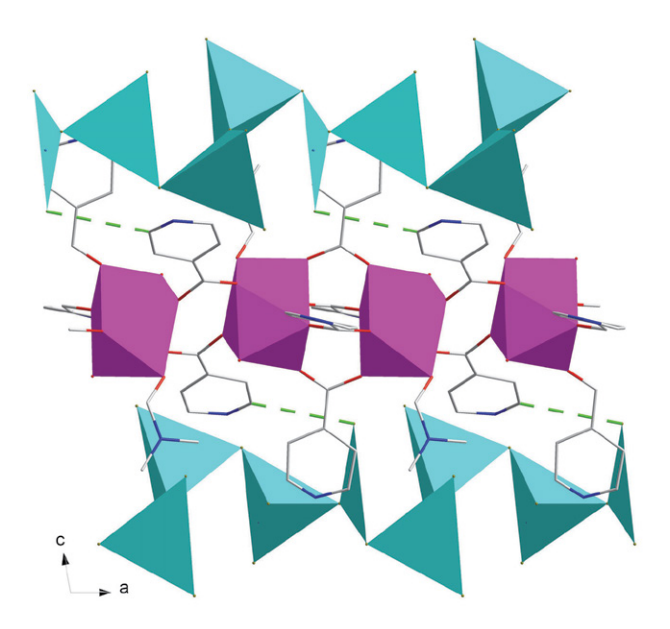


Fig. 8: A 2-D supramolecular layer in complex **2** with the green dashed lines representing hydrogen bonding interactions. The turquiose and pink are Hg- and Nd-centered polyhedra, respectively.

emissions. As a result, it is supposed that both title complexes should exhibit photoluminescence emissions because they possess lanthanide and mercury ions simultaneously. Based on this consideration, the powder samples of both title complexes were applied to conduct the photoluminescence experiments at room temperature. The results of the photoluminescence experiments of both title complexes are presented in Fig. 10 and Fig. 11. As for complex 1, when it was excited by the UVA light of 386 nm, it exhibited the UVB photoluminescence with an emission band locating at 312 nm, as displayed in Fig. 10. The photoluminescence emission originates from the characteristic emissions of the 4f electron intrashell transitions of the Gd³⁺ ions in complex 1.⁴³ UVB includes the wavelength 280-320 nm of the spectrum therefore, complex 1 is a potential UVB photoluminescence emission material. With regard to complex 2, the photoluminescence absorption

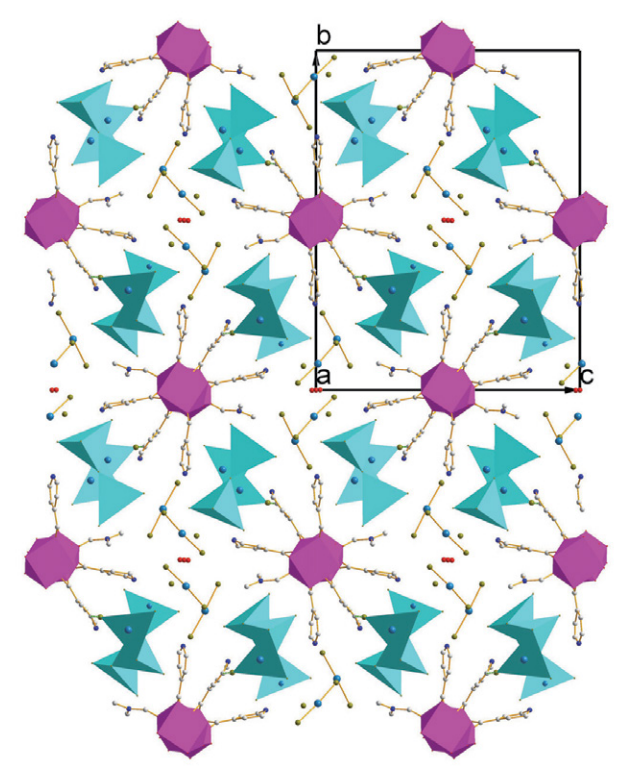


Fig. 9: The packing structure of complex **2**. The turquiose and pink are Hg- and Nd-centered polyhedra, respectively.

is located in the span of 480 nm \sim 550 nm with an adsorption peak at 496 nm. When it was excited by the 496 nm light, complex 2 exhibits red photoluminescence emissions in the span of 620 nm \sim 900 nm with four emission bands locating at 682, 745, 823 and 885 nm, of which 745 nm is the strongest one, as shown in Fig. 11. These photoluminescence emission bands come from the characteristic emissions of the 4f electron intrashell transitions of the Nd³+ ions in compound 2. As presented in Fig. 12, compound 2 has CIE chromaticity coordinates (0.7142, 0.2857) in the red region and its CCT is 138224 K. As a result, complex 2 is supposed to be a potential red light photoluminescent material.

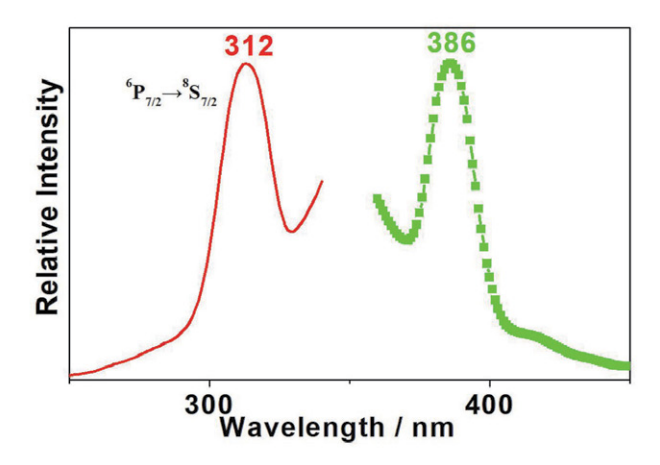


Fig. 10: Solid state photoluminescence spectra of complex 1 with the green and red lines representing excitation and emission spectra, respectively.

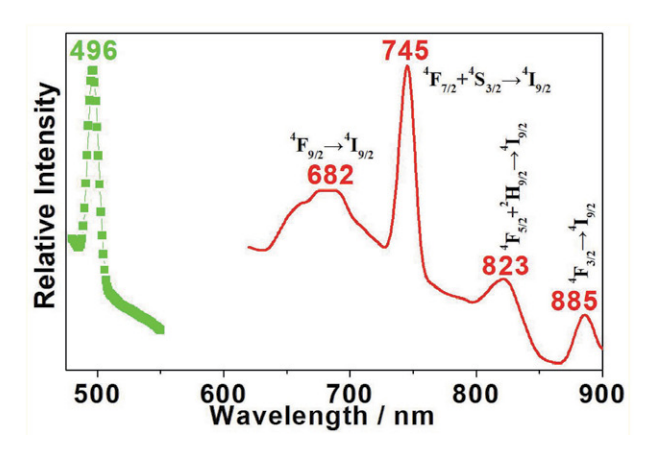


Fig. 11: Solid state photoluminescence spectra of complex **2** with the green and red lines representing excitation and emission spectra, respectively.

As for lanthanide materials, their photoluminescence, magnetic and catalytic properties have been widely explored so far, but their semiconductive properties have been relatively rarely investigated. Considering this reason and in order to more deeply explore the photophysical performances of compounds 1 and 2, their solid state UV/Vis diffuse reflection measurements were carried out with a finely ground powder sample at room temperature. The solid state UV/Vis diffuse reflectance spectra data for complexes 1 and 2 were processed with the famous Kubelka-Munk formula $\alpha/S = (1-R)^2/2R$, where α refers to the absorption coefficient, S is the scattering coefficient, R is the reflection coefficient. The converted solid state UV/Vis diffuse reflectance spectra are given in Figs. 13 and 14 for complexes 1 and 2, respectively. The semiconductive bandgaps for complexes 1 and 2 can be found by virtue of the straight line extrapolation technique from the maximum absorption edges of the α /S versus energy diagrams. Based on such a technique, the semiconductive bandgaps for complexes 1 and 2 can be found to be 3.12 eV and 3.23 eV,

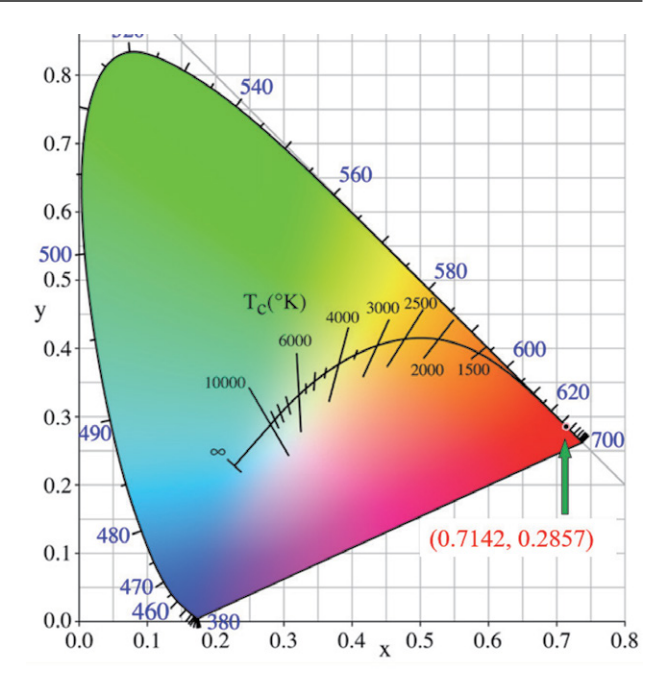


Fig. 12: The CIE diagram of complex 2.

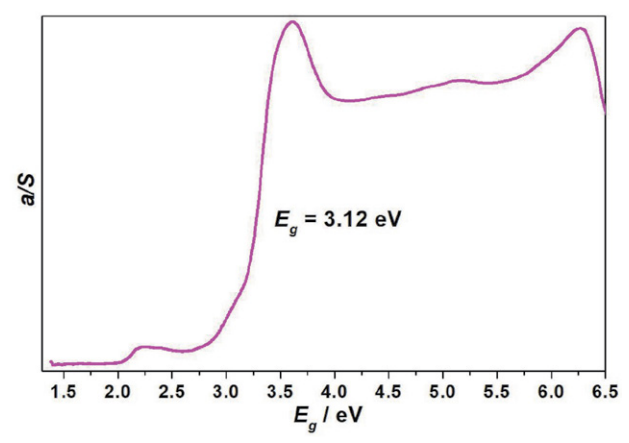


Fig 13: The UV-vis diffuse reflectance diagram measured with a solid state sample of complex 1.

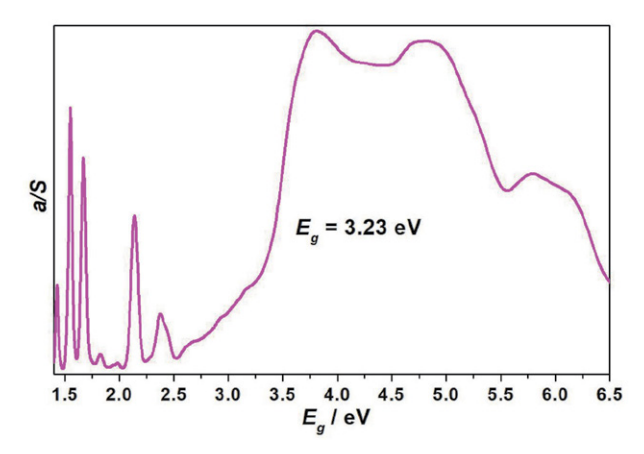


Fig 14: The UV-vis diffuse reflectance diagram measured with a solid state sample of complex **2**.

respectively. Furthermore, the solid state UV/Vis diffuse reflectance curves of complexes 1 and 2 reveal that the maximum absorption edges are not very steep, which indicates that both of them should go through an indirect transition process. ⁴⁵ As a result, complexes 1 and 2 are potentially a candidate for wide bandgap semiconductive materials.

4. Conclusions

In brief, we have synthesized two new lanthanide mercury halide compounds each possessing distinct crystal structures: one exhibits a 2-D layer-like structure, while the other features a 1-D chain-like structure. One compound has a ultraviolet upconversion photoluminescence emission, while the other shows red photoluminescence. These emissions originate from the characteristic emissions of the 4f electron intrashell transitions of the ${}^{6}P_{7/2} \rightarrow {}^{8}S_{7/2}$ of the Gd³⁺ ions and the ${}^{4}F_{9/2} \rightarrow {}^{4}I_{9/2}$, ${}^{4}F_{7/2}$ + ${}^{4}S_{3/2} \rightarrow {}^{4}I_{9/2}, {}^{4}F_{5/2} + {}^{2}H_{9/2} \rightarrow {}^{4}I_{9/2}, {}^{4}F_{3/2} \rightarrow {}^{4}I_{9/2}$ of the Nd³⁺ ions. The neodymium compound possesses CIE chromaticity coordinates of (0.7142, 0.2857) and a CCT of 138224 K. Solid-state UV/Vis diffuse reflectance spectra revealed that they are potential wide bandgap semiconductive materials. Further investigations on the relationship between the crystal structures and the physicochemical properties in this field are in progress in our lab.

Acknowledgements

We greatly thank for the financial support of the National Natural Science of Foundation of China (22265014, 22262015), the Natural Science of Foundation of Jiangxi Province (20242BAB26034, 20224BAB204008, 20212BAB213020, 20232BCJ23026), Key Laboratory of Jiangxi Province for Special Optoelectronic Artificial Crystal Materials (20242BCC32037), as well as the Science and Technology Project of Jiangxi Provincial Department of Education (GJJ2201602).

Supplementary Material

Crystallographic data for the structure reported in this paper have been deposited with the Cambridge Crystallographic Data Centre as supplementary publication No. CCDC 2377406 and 2377012 for complexes 1 and 2, respectively. Copies of the data can be obtained free of charge on application to CCDC, 12 Union Road, Cambridge CB2 1EZ, UK (fax: (44) 1223 336-033; e-mail: deposit@ccdc.cam.ac.uk).

5. References

 M. Rakhmanova, T. Sukhikh, E. Kovalenko, CrystEngComm 2024, 26, 3954–3963. DOI:10.1039/D4CE00375F

- A. Mortis, R. Anwander, Eur. J. Inorg. Chem. 2024, 27, e202400127. DOI:10.1002/ejic.202400127
- E. A. Sanzhenakova, K. S. Smirnova, I. P. Pozdnyakov, E. V. Lider, J. Struct. Chem. 2024, 65, 786–797.
 DOI:10.1134/S0022476624040140
- R. Huo, T. Zhang, G. Zeng, C. Wang, Y. H. Xing, F. Y. Bai, *Chinese J. Chem.* 2024, 42, 283–293.
 DOI:10.1002/cjoc.202300448
- M. O. Savchuk, O. O. Litsis, N. S. Kariaka, V. O. Trush, V. V. Dyakonenko, S. S. Smola, J. A. Rusanova, T. Y. Sliva, S. V. Shishkina, V. M. Amirkhanov, *Inorg. Chim. Acta* 2024, 559, 121783. DOI:10.1016/j.ica.2023.121783
- C. Chen, C. Lu, B. Zhao, J. Org. Chem. 2023, 88, 16391–16399.
 DOI:10.1021/acs.joc.3c01905
- B. Alnami, J. G. C. Kragskow, J. K. Staab, J. M. Skelton, N. F. Chilton, *J. Am. Chem. Soc.* 2023, 145, 13632–13639.
 DOI:10.1021/jacs.3c01342
- 8. D. I. Galimov, S. M. Yakupova, R. G. Bulgakov, *J. Photochem. Photobio. A* **2023**, 438, 114559.
 - DOI:10.1016/j.jphotochem.2023.114559
- Y. F. Wang, X. Gao, C. S. Cao, S. M. Li, Z. L. Wu, *Inorg. Chim. Acta* 2023, 546, 121327. DOI:10.1016/j.ica.2022.121327
- Y. W. Wang, M. H. Yang, Z. C. Cui, H. H. Zeng, X. Zhang, J. Q. Shi, T. F. Cao, X. L. Fan, J. Mater. Sci. 2023, 58, 268–280.
 DOI:10.1007/s10853-022-08024-8
- H. Reuter, M. Boeltken, M. Horstmann, M. Haase, Crystals 2023, 13, 1043. DOI:10.3390/cryst13071043
- 12. K. Wydra, V. Kinzhybalo, J. Lisowski, *Dalton Trans.* **2023**, *52*, 11992–12001. **DOI:**10.1039/D3DT01948A
- L. X. Meng, J. L. Wang, Y. Zhang, B. X. Zhou, J. J. Shi, K. Xiao, Sensor. Actuat. B- Chem. 2024, 414, 135897.
 DOI:10.1016/j.snb.2024.135897
- C. Yu, Y. Shan, J. Zhu, D. Sun, X. Zheng, N. Zhang, J. Hou, Y. Fang, N. Dai, Y. Liu, *Materials* 2024, 17, 1864.
 DOI:10.3390/ma17081864
- Y. Tian, H. Luo, M. Chen, C. Li, S. V. Kershaw, R. Zhang, A. L. Rogach, *Nanoscale* **2023**, *15*, 6476–6504.
 DOI:10.1039/D2NR07309A
- Y. Selmani, H. Labrim, R. E. L. Bouaydi, L. Bahmad, *Phys. B* 2022, 644, 414204. DOI:10.1016/j.physb.2022.414204
- H. Song, S. Y. Eom, G. Kim, Y. S. Jung, D. Choi, G. S. Kumar, J. H. Lee, H. S. Kang, J. Ban, G. W. Seo, *Commun. Mater.* 2024, 5, 60. DOI:10.1038/s43246-024-00499-z
- S. Padwal, R. Wagh, J. Thakare, R. Patil, *Appl. Phys. A* 2024, 130, 34. DOI:10.1007/s00339-023-07202-y
- Y. Xie, F. Guo, W. Tong, H. Chang, *Inorg. Chem.* 2024, 63, 4160–4167. DOI:10.1021/acs.inorgchem.3c03969
- S. Kukreti, S. Ramawat, A. Dixit, *Phys. Stat. Sol. B* 2023, 260, 2200524.
- 21. Y. L. Liu, Y. X. Zhao, J. H. Zhang, Y. Ye, Q. Q. Sun, *J. Solid State Chem.* **2022**, *313*, 123332. **DOI**:10.1016/j.jssc.2022.123332
- S. Wang, Y. Li, B. Wang, J. Chem. Res. 2021, 45, 934–941.
 DOI:10.1177/17475198211032835
- 23. L. B. Zhu, F. Li, M. L. Sun, Y. Y. Qin, Y. G. Yao, *Chinese J. Struct. Chem.* **2021**, *40*, 1031–1038.
- 24. J. F. Zhang, J. J. Wu, G. D. Tang, J. Y. Feng, F. M. Luo, B. Xu, C.

- Zhang, Sensor Actuat. B-Chem. **2018**, 272, 166–174. **DOI:**10.1016/j.snb.2018.05.121
- N. N. Pang, D. X. Lin, Z. Y. Zhan, X. D. Ding, T. T. Shi, Q. X. Meng, P. Y. Liu, W. G. Xie, *Mat. Sci. Semicon. Proc.* 2022, 145, 106639. DOI:10.1016/j.mssp.2022.106639
- F. E. Özbek, M. Sertçelik, M. Yüksek, G. Ugurlu, A. M. Tonbul,
 H. Necefoglu, T. Hökelek, *J. Fluoresc.* 2019, 29, 1265–1275.
 DOI:10.1007/s10895-019-02440-x
- X. Zhang, W.-T. Chen, J. Mol. Struct. 2024, 1301, 137257.
 DOI:10.1016/j.molstruc.2023.137257
- H.-D. Liu, Y.-Y. Xu, X.-Y. Shao, L.-H. Zeng, W.-T. Chen, C. Liu, S.-P. Dai, C.-W. Pan, *J. Mol. Struct.* 2024, 1305, 137762.
 DOI:10.1016/j.molstruc.2024.137762
- H.-D. Liu, X.-Y. Shao, L.-H. Zeng, Y.-Y. Xu, C. Liu, S.-P. Dai,
 C.-W. Pan, W.-T. Chen, J. Porphyr. Phthalocya. 2024, 28,
 157–165. DOI:10.1142/S108842462450010X
- P. Makuła, M. Pacia, W. Macyk, J. Phys. Chem. Lett. 2018, 9, 6814–6817. DOI:10.1021/acs.jpclett.8b02892
- 31. H.-H. Lee, I.-H. Park, S. S. Lee, *Inorg. Chem.* **2014**, *53*, 4763–4769. **DOI**:10.1021/ic500594f
- N.-H. Hu, K. Aoki, A. O. Adeyemo, G. N. Williams, *Inorg. Chim. Acta* 2022, 333, 63–71.
- J.-L. Song, J.-G. Mao, H.-Y. Zeng, Z.-C. Dong, Eur. J. Inorg. Chem. 2004, 38–543. DOI:10.1002/ejic.200300554
- Y. J. Nie, Y. H. Deng, H. X. Guo, S. M. Ying, *Chinese J. Struct. Chem.* 2020, 39, 1029–1034. DOI:10.1002/cjoc.202190052
- M. T. Kaczmarek, R. Jastrzab, M. Kubicki, M. Gierszewski, M. Sikorski, *Inorg. Chim. Acta* 2015, 430, 108–113.
 DOI:10.1016/j.ica.2015.02.026

- H.-D. Liu, X.-Y. Shao, Y.-Y. Xu, W.-T. Chen, Ch. Liu, S.-P. Dai,
 C.-W. Pan, *Acta Chim. Slov.* 2024, 71, 380–387.
 DOI:10.17344/acsi.2024.8661
- P. Nockemann, G. Meyer, Z. Anorg. Allg. Chem. 2003, 629, 123–128. DOI:10.1002/zaac.200390003
- 38. X. Zhang, W. Chen, *J. Mol. Struct.* **2024**, *1301*, 137257. **DOI:**10.1016/j.molstruc.2023.137257
- S.-C. Chen, H.-H. Hsueh, C.-H. Chen, C. S. Lee, F.-C. Liu, I. J. B. Lin, G.-H. Lee, S.-M. Peng, *Inorg. Chim. Acta* 2009, 362, 3343–3350. DOI:10.1016/j.ica.2009.03.014
- W.-J. Zhang, Y.-Y. Xu, L.-J. Wei, J.-Y. Lin, W.-T. Chen, W.-S. Lin, *Inorg. Chim. Acta* 2023, 547, 121328.
 DOI:10.1016/j.ica.2022.121328
- I. V. Kalinovskaya, A. Y. Mamaev, V. E. Karasev, Russ. J. Gen. Chem. 2011, 81, 1407–1410.
 DOI:10.1134/S1070363211070012
- D.-Y. He, L.-J. Wei, Y.-Y. Xu, Z.-G. Luo, W.-T. Chen, W.-S. Lin, *J. Iran. Chem. Soc.* 2023, 20, 1323–1331.
 DOI:10.1007/s13738-023-02757-2
- V. Singh, G. Sivaramaiah, N. Singh, J. L. Rao, P. K. Singh, M. S. Pathak, D. A. Hakeem, *Optik* 2018, 158, 1227–1233.
 DOI:10.1016/j.ijleo.2017.12.185
- 44. S. Insiripong, S. Kaewjeang, U. Maghanemi, H. J. Kim, N. Chanthima, J. Kaewkhao, *Appl. Mechan. Mater.* **2014**, 548–549, 124–128.
 - DOI:10.4028/www.scientific.net/AMM.548-549.124
- S. F. M. Schmidt, C. Koo, V. Mereacre, J. Park, D. W. Heermann, V. Kataev, C. E. Anson, D. Prodius, G. Novitchi, R. Klingeler, A. K. Powell, *Inorg. Chem.* 2017, 56, 4796–4806.
 DOI:10.1021/acs.inorgchem.6b02682

Povzetek

S solvotermalno sintezo smo sintetizirali dve novi spojini z lantanoidi in živim srebrom ter izonikotinsko kislino kot ligandom in sicer $[Gd(\mu_2-HIA)_2(\mu_3-IA)(H_2O)_2(HgCl_2)]_n(nHgCl_4)\cdot 3nH_2O$ (1) (HIA = izonikotinska kislina) in $\{[Nd(\mu_2-HIA)_3(DMF)(H_2O)]_n\}[(Hg_4Br_{11})_n](2HgBr_2)(nBr)\cdot nH_3O$ (2). Obe spojini smo karakterizirali z monokristalno rentgensko difrakcijo. Spojina 1 ima dvodimenzionalno (2-D) plastovito strukturo, međtem ko ima spojina 2 enodimenzionalno (1-D) verižno zgradbo. Lantanoidni ioni v obeh spojinah so osemštevno koordinirani v obliki kvadratne antiprizme, međtem ko ima živosrebrov ion različne koordinacijske motive. Spojina 1 kaže ultravijolično fotoluminiscenco, međtem ko ima spojina 2 rdečo fotoluminiscenco. Razlog za fotoluminiscenčno emisijo so karakteristicni prehodi 4*f* elektronov $^6P_{7/2} \rightarrow ^8S_{7/2}$ Gd³⁺ ionov v spojini 1 in $^4F_{9/2} \rightarrow ^4I_{9/2} \rightarrow ^4F_{9/2} \rightarrow ^4I_{9/2} \rightarrow ^4I_{9/2} \rightarrow ^4I_{9/2} \rightarrow ^4I_{9/2} \rightarrow ^4I_{9/2} \rightarrow ^4I_{9/2}$ prehodi Nd³⁺ ionov v spojini 2. Spojina 2 ima barvne koordinate (0.7142, 0.2857) CIE (Commission Internationale de l'Éclairage) in vrednost CCT (korelirana barvna temperatura) 138,224 K. Iz UV/Vis spektrov v trdnem stanju smo izračunali polprevodniške širine prepovedanega pasu, ki znašajo 3.12 eV in 3.23 eV. Elementna analiza in FT-IR spektri potrjujejo čistost obeh spojin.



Except when otherwise noted, articles in this journal are published under the terms and conditions of the Creative Commons Attribution 4.0 International License